

# Precise dating of deglacial Laptev Sea sediments via $^{14}\text{C}$ and authigenic $^{10}\text{Be}/^9\text{Be}$ – assessing local $^{14}\text{C}$ reservoir ages

Arnaud Nicolas<sup>1,2</sup>, Gesine Mollenhauer<sup>1,2,3</sup>, Johannes Lachner<sup>4</sup>, Konstanze Stübner<sup>4</sup>, Maylin Malter<sup>1</sup>, Jutta Wollenburg<sup>1</sup>, Hendrik Grotheer<sup>1,3</sup>, Florian Adolphi<sup>1,2</sup>

<sup>1</sup>Alfred Wegener Institute, Bremerhaven, Germany

<sup>2</sup>Department of Geosciences, University of Bremen, Bremen, Germany

<sup>3</sup>MARUM-Center for Marine Environmental Sciences, University of Bremen, Bremen, Germany

<sup>4</sup>Helmholtz-Zentrum Dresden-Rossendorf, Dresden, Germany

Correspondence: Arnaud Nicolas (arnaud.nicolas@awi.de) and Florian Adolphi (florian.adolphi@awi.de)

## Abstract

Establishing accurate chronological frameworks is imperative for reliably identifying lead-lag dynamics within the climate system and enabling meaningful inter-comparisons across diverse paleoclimate proxy records over long time periods. Robust age models provide a solid temporal foundation for establishing correlations between paleoclimate records. One of the primary challenges in constructing reliable radiocarbon-based chronologies in the marine environment is to determine the regional marine radiocarbon reservoir age correction. Calculations of the local marine reservoir effect ( $\Delta R$ ) can be acquired using  $^{14}\text{C}$ -independent dating methods, such as synchronization with other well-dated archives. The cosmogenic radionuclide  $^{10}\text{Be}$  offers such a synchronization tool. Its atmospheric production rate is controlled by the global changes in the cosmic ray influx, caused by variations in solar activity and geomagnetic field strength. The resulting fluctuations in the meteoric deposition of  $^{10}\text{Be}$  are preserved in sediments and ice cores and can thus be utilized for their synchronization. In this study, for the first time, we use the authigenic  $^{10}\text{Be}/^9\text{Be}$  record of a Laptev Sea sediment core for the period 8-14 kyr BP and synchronize it with the  $^{10}\text{Be}$  records from absolutely dated ice cores. Based on the resulting absolute chronology, a benthic  $\Delta R$  value of  $+345 \pm 60$   $^{14}\text{C}$  years was estimated for the Laptev Sea, which corresponds to a marine reservoir age of  $848 \pm 90$   $^{14}\text{C}$  years. The  $\Delta R$  value was used to refine the age-depth model for core PS2458-4, establishing it as a potential reference chronology for the Laptev Sea. We also compare the calculated  $\Delta R$  value with modern estimates from the literature and discuss its implications for the age-depth model.

## 1 Introduction

Paleoclimate reconstructions can provide useful information about the dynamics of the climate system under different boundary conditions. Investigating how the climate variations propagate in space and time can provide important information about the underlying driving mechanisms (Adolphi et al., 2018; Czymzik et al., 2016b, a; Reinig et al., 2021). To correctly assess regional variations and spatio-temporal patterns in climate fluctuations, it is crucial to construct precise chronological frameworks. These frameworks serve as the temporal backbone for establishing correlations between paleoclimate records derived from marine, terrestrial, and ice-core archives. However, uncertainties in chronologies across different paleoclimate records often hinder the precise assessment of paleoclimate dynamics involving multiple records from different sites and archives (Southon, 2002).

One of the key challenges for constructing precise chronologies in the marine realm is to estimate the regional marine radiocarbon reservoir age correction, especially in polar regions (Alves et al., 2018; Heaton et al., 2023).

46 For constructing an age-depth model using  $^{14}\text{C}$  dates of marine samples, it is crucial to include a precise marine  
47 reservoir age (MRA). The MRA is the radiocarbon age difference between a marine sample and its contemporary  
48 atmosphere (Stuiver et al., 1986). According to the most recent radiocarbon calibration curve, Marine20, the global  
49 average marine reservoir age is approximately 500  $^{14}\text{C}$  years during the Holocene period (0 - 11.6 kyr BP) (Heaton  
50 et al., 2020). However, regional differences in ocean-atmosphere exchange and internal ocean mixing can result  
51 in large regional deviations from this global mean (Heaton et al., 2023). Therefore, the local marine reservoir  
52 effect,  $\Delta R$  was introduced and is defined as the difference between the regional and the modelled global marine  
53 reservoir ages (Reimer and Reimer, 2001; Stuiver et al., 1986).

54

55 There is only one study that has provided modern MRA estimates for the Laptev Sea (Bauch et al., 2001). In this  
56 study, the MRAs range from  $295 \pm 45$  to  $860 \pm 55$   $^{14}\text{C}$  years, with a mean value of  $451 \pm 72$   $^{14}\text{C}$  years. Estimates  
57 for MRA from the early deglaciation (~15 kyr BP) to the Holocene period for creating reliable deglacial  
58 chronologies in the Laptev Sea are so far not available.

59

60 In order to provide estimates of the local  $\Delta R$  back in time the samples must be independently dated by other means  
61 than  $^{14}\text{C}$ . This can for example be achieved by synchronization to other well-dated archives. Cosmogenic  
62 radionuclides such as  $^{10}\text{Be}$  and provide such a synchronization tool (Adolphi et al., 2018; Adolphi and Muscheler,  
63 2016; Czymzik et al., 2018, 2020; Muscheler et al., 2014; Southon, 2002).

64

65 The cosmogenic radionuclides Beryllium-10 ( $^{10}\text{Be}$ , half-life =  $1.387 \pm 0.012$  Myr) (Chmeleff et al., 2010;  
66 Korschinek et al., 2010) and Carbon-14 ( $^{14}\text{C}$ , half-life =  $5.700 \pm 0.03$  kyr) (Audi et al., 2003) are mainly produced  
67 in Earth's upper atmosphere in a particle cascade that is triggered when galactic cosmic rays interact with atoms  
68 in the atmosphere (Lal and Peters, 1967; Dunai and Lifton, 2014). The flux of these cosmic rays reaching Earth  
69 is controlled by variations in the heliomagnetic and geomagnetic shielding (Lal and Peters, 1967; Masarik and  
70 Beer, 1999) During periods of higher solar activity and/or geomagnetic field strength, production rates of  $^{10}\text{Be}$   
71 and  $^{14}\text{C}$  are decreased, whereas the production rates are higher during reduced solar activity and/or lower magnetic  
72 field strength. The production rates of both cosmogenic radionuclide isotopes co-vary globally due to these  
73 external processes.

74

75 Following production in the atmosphere,  $^{14}\text{C}$  oxidizes to  $^{14}\text{CO}_2$ , enters the global carbon cycle and is incorporated  
76 in environmental archives such as tree-rings, foraminifera, or speleothems. Annually, gigatons of carbon are  
77 exchanged between the Earth's active reservoirs of the atmosphere, biosphere and the ocean, within the global  
78 carbon cycle. Carbon is recycled and reused within these reservoirs and some reservoirs such as the deep ocean  
79 can take hundreds of years to recycle carbon back to the atmosphere. The resulting heterogenous distribution of  
80 radiocarbon among the different reservoirs stress the importance to understand and determine precise reservoir  
81 ages.

82

83 In the atmosphere, the production of  $^{10}\text{Be}$  in the more stably layered stratosphere is higher than in the troposphere.  
84 About 63 % of  $^{10}\text{Be}$  is produced in the stratosphere, 30 % in the tropical and subtropical troposphere together and  
85 7 % in the polar troposphere (Adolphi et al., 2023; Poluianov et al., 2016).  $^{10}\text{Be}$  is adsorbed onto aerosol particles,

86 mixed during about 1-yr residence time in the stratosphere, and is then transported and deposited on Earth's  
87 surfaces through wet and dry deposition (Raisbeck et al., 1981; Zheng et al., 2023). The  $^{10}\text{Be}$  production rates are  
88 highest in the high-latitude stratosphere due to the weaker shielding of the cosmic ray flux by the Earth's magnetic  
89 field. However, the highest  $^{10}\text{Be}$  fluxes to Earth's surface are recorded in mid-latitudes because of the strong  
90 regional exchange between stratosphere and troposphere and high precipitation rates leading to strong aerosol  
91 scavenging (Heikkilä et al., 2013). Non-production processes such as variations in mixing, transport and  
92 deposition of  $^{10}\text{Be}$  and  $^{14}\text{C}$  can complicate the reconstruction of cosmogenic radionuclide production rates from  
93 paleoenvironmental archives. However, common variations in both cosmogenic radionuclide records are  
94 considered to represent the cosmogenic radionuclide production signal, due to their common production  
95 mechanism and different chemical behavior (Lal and Peters, 1967; Muscheler et al., 2008).  $^{10}\text{Be}$  production rate  
96 changes are relatively well-known from independently dated ice-core records (Finkel and Nishiizumi, 1997; Yiou  
97 et al., 1997), and this can serve as a synchronization target for other records of  $^{10}\text{Be}$  production rate changes.

98  
99 In order to obtain reliable records of  $^{10}\text{Be}$ -production rate changes from marine sediments, the effects of variable  
100 sedimentation rates and particle scavenging must be accounted for, which can be efficiently achieved by  
101 measuring authigenic  $^{10}\text{Be}/^9\text{Be}$  (Bourles et al. 1989). The stable isotope  $^9\text{Be}$  is a trace component in all continental  
102 rocks. It is released by weathering of silicate rocks and transported to the ocean mainly by rivers (von  
103 Blanckenburg et al., 2015).  $^9\text{Be}$  (and to a lesser extent meteoric  $^{10}\text{Be}$ ) is introduced into the ocean in its dissolved  
104 form where it is mixed with dissolved  $^{10}\text{Be}$  of ocean water (mainly derived from atmospheric fallout, see above).  
105 Since Be is particle reactive in seawater, dissolved  $^{10}\text{Be}/^9\text{Be}$  is incorporated in marine authigenic phases as  
106 amorphous coating on sediment or it can be preserved in authigenic Fe-Mn oxyhydroxides (von Blanckenburg  
107 and Bouchez, 2014). Therefore, in marine sediment the authigenic  $^{10}\text{Be}/^9\text{Be}$  ratio reflects the isotope ratio of  
108 dissolved Be of the overlying water column at the time of sediment deposition (Bourles et al., 1989; von  
109 Blanckenburg and Bouchez, 2014).

110  
111 If the riverine input of  $^9\text{Be}$  remains relatively constant,  $^9\text{Be}$  and  $^{10}\text{Be}$  are well-mixed (i.e., at sites >200 km from  
112 the coast) (Wittmann et al., 2017), and the mixing of prevalent water-masses does not change, then authigenic  
113  $^{10}\text{Be}/^9\text{Be}$  should primarily reflect changes in the cosmogenic production rates of  $^{10}\text{Be}$ . In the Arctic Ocean, the  
114 spatial patterns of  $^{10}\text{Be}/^9\text{Be}$  in the water column are more heterogeneous than most other open ocean settings  
115 because of the mixing of Atlantic waters with  $^{10}\text{Be}/^9\text{Be}$  values of  $5 - 10 \times 10^{-8}$  and Arctic Rivers with  $^{10}\text{Be}/^9\text{Be}$   
116 values of  $0.3 - 1.5 \times 10^{-8}$  (Frank et al., 2009).

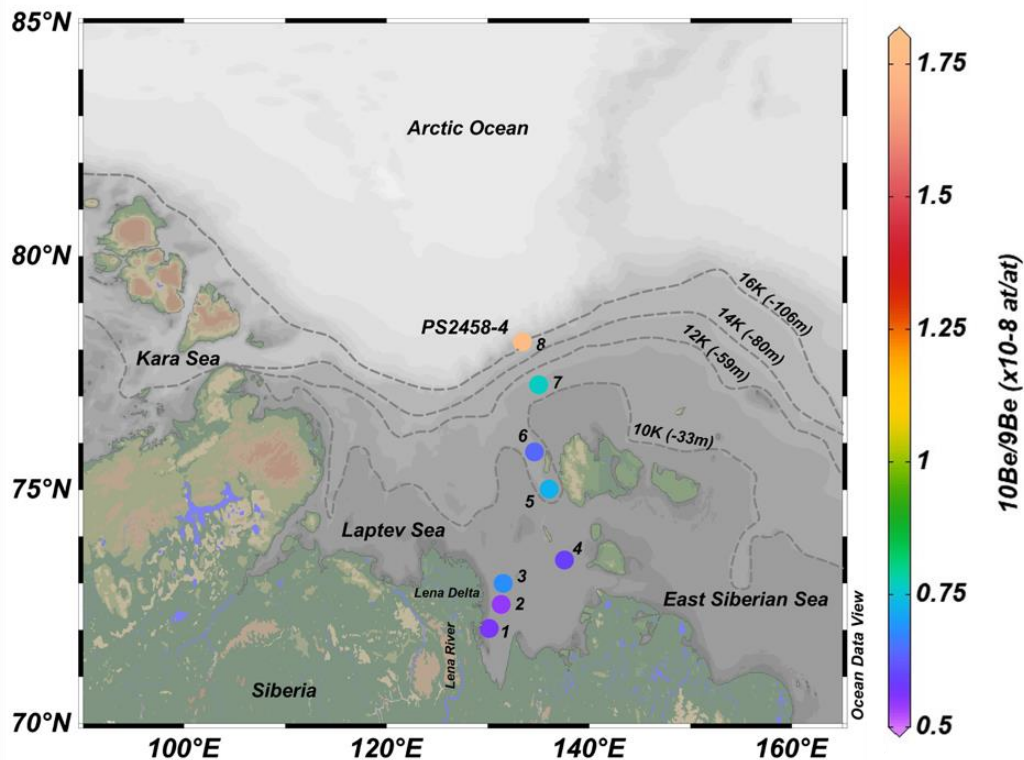
117  
118 The aim of this study is to explore the use of an authigenic  $^{10}\text{Be}/^9\text{Be}$  of a Laptev Sea sediment core for its  
119 synchronization to  $^{10}\text{Be}$ -records from absolutely dated ice cores. Using this result, we aim to infer the the local  
120 marine reservoir effect,  $\Delta R$  for the Laptev Sea during the deglaciation. This is the first study to exploit variations  
121 in  $^{10}\text{Be}$  production rates from Arctic marine sediments for stratigraphic purposes.

122  
123  
124  
125  
126  
127

128 **2 Materials and methods**

129 **2.1 Sediment core location and initial chronology**

130 The sediment core PS2458-4 measured for  $^9\text{Be}$  and  $^{10}\text{Be}$  in this study, was retrieved in 1994 from the eastern  
131 Laptev Sea continental margin (78°10.0'N, 133°23.9'E) at a water depth of 983 m (Fütterer, 1994) and  
132 approximately about 518 km from the Lena Delta (Fig. 1). The 8 m long core consists of very dark olive-grey silty  
133 clay of dominantly terrigenous origin (Fütterer, 1994). This core consists of a continuous high-sedimentation-rate  
134 (77 cm /kyr) sequence representing the deglaciation period between approximately 16.5 and 9.3 kyr BP, followed  
135 by a lower-sedimentation-rate (27 cm /kyr) early Holocene sequence (Fahl and Stein, 2012). A first chronology  
136 of core PS2458-4 was established by accelerator mass spectrometry (AMS)  $^{14}\text{C}$  dating of calcareous foraminifera,  
137 bivalves and wood samples for the sediment interval between 201 and 667 cm, corresponding to a time interval  
138 between approximately 8.8 and 14.3 kilo-calendar years BP (kyr BP) (Spielhagen et al., 2005). To improve the  
139 existing age-depth model, 7 new AMS  $^{14}\text{C}$  dates from mixed benthic foraminifera were used in combination with  
140 7  $^{14}\text{C}$  dates from mixed benthic foraminifera and bivalves from Spielhagen et al. (2005) and an initial age-model  
141 was derived using OxCal4.4 (Ramsey, 2009) (see Table 2). The mixed bivalve species used in Spielhagen et al.  
142 (2005) were described as *Thyasira* sp. and *Yoldiella* sp (Table S1). Both bivalve species typically occur in cold  
143 water environments at continental margins and in areas of limited food supply, as is the Laptev Sea continental  
144 margin. Concerning the mixed benthic foraminifera species, usually epibenthic species such as *Lobatula lobatula*  
145 are preferred. Since this latter species is rare in our sediment samples, other species such as: *Cassidulina*  
146 *neoteretis*, *Islandiella helenae* and *Islandiella norcrossi* were selected for radiocarbon dating. In the Arctic Ocean  
147 all these species live close to the sediment surface (Wollenburg and Kuhnt, 2000; Wollenburg and Mackensen,  
148 1998) and reflect the carbon and oxygen isotope record of the bottom water in their shells. The marine  $^{14}\text{C}$  dates  
149 were calibrated with the Marine20 curve (Heaton et al., 2020). An average local marine reservoir effect ( $\Delta\text{R}$ ) value  
150 of  $-110 \pm 28$   $^{14}\text{C}$  years was used based on the nearest modern values from Bauch et al. (2001) available from the  
151 online database: <http://calib.org/marine/>. This chronology provides the initial basis for the stratigraphic fine-tuning  
152 using  $^{10}\text{Be}/^9\text{Be}$  as described below.



154 **Figure 1: Map of the Laptev Sea shelf showing the location of core PS2458-4 with core-top  $^{10}\text{Be}/^9\text{Be}$  concentration**  
 155 **(numbered colored circle 8) and  $^{10}\text{Be}/^9\text{Be}$  concentrations of modern surface sediments (numbered colored circles 1-7).**  
 156 **The dashed lines represent the reconstructed coastline extent at 4 different time periods (where 16K=16 kyr BP) with**  
 157 **corresponding water depth values in meters shown in brackets (Klemann et al., 2015) . The Map was created using**  
 158 **Ocean Data View (Schlitzer, 2016)**

## 159 2.2 Modern surface sediment samples from Laptev Sea

160 Seven modern surface sediment samples collected in the Laptev Sea were also included in the analysis (Figure 1,  
 161 Table 1). Surface sediments with sample IDs 1 to 6 were collected during the Transdrift expeditions I and II in  
 162 1993 and 1994 using Van Veen grabs and large spade box corer (Kassens and Dmitrenko, 1995; Kassens and  
 163 Karpiy, 1994). Sediment sample from core PS2728-2 with ID number 7 was recovered in 1995 with a large  
 164 rectangular box sampler during the Arctic Expedition ARK-XI/1 (Rachor, 1997). The sediment samples used in  
 165 this study are distributed along a transect from near to the Lena Delta towards the open ocean near the shelf break,  
 166 close to where core PS2458-4 was retrieved.

## 167 2.3 Sample preparation and measurements

168 Fifty-four sediment samples were selected along core PS2458-4 and processed for Be isotope analysis at the  
 169 Alfred Wegener Institute in Bremerhaven (Germany). According to the initial radiocarbon-based age model, the  
 170 selected samples covered three large cosmogenic radionuclide production rate swings, as evidenced by ice core  
 171  $^{10}\text{Be}$  and tree-ring  $^{14}\text{C}$  records (e.g., Adolphi and Muscheler, 2016), that occurred between 8.5 and 11.5 kyr BP.  
 172 The leaching of the authigenic Fe-Mn oxyhydroxides phase followed Gutjahr et al. (2007) with minor  
 173 modifications. Sediment samples were freeze-dried, homogenised and ~1 g of sediment was treated with 1 M  
 174 NaOAc and adjusted with HOAc to pH 4 to dissolve carbonates which were discarded. Subsequently, the  
 175 sediments were leached using 0.04 M hydroxylamine ( $\text{NH}_2\text{OH}\cdot\text{HCl}$ ) in 15% HOAc at 95 °C for 4 h. We did not

176 leach the exchangeable fraction as proposed by Gutjahr et al. (2007) as this contained less than 1 % of the Be  
177 leached in the hydroxylamine fraction with a very similar  $^{10}\text{Be}/^9\text{Be}$  ratio. An aliquot from the resulting leaching  
178 solution was sampled for stable  $^9\text{Be}$  measurements using an Atomic Emission Spectrophotometer at the Alfred  
179 Wegener Institute in Bremerhaven, Germany (Thermo Fisher Scientific Inc., ICP-OES-iCAP7400), with an  
180 internal Yttrium standard and standard addition. The remaining  $^{10}\text{Be}$  aliquot solution was spiked with a precisely  
181 weighed amount of  $^9\text{Be}$ -carrier (200, 300 or 500  $\mu\text{L}$  of 1000 mg/L carrier solution, LGC 998969-73,  $^{10}\text{Be}/^9\text{Be} =$   
182  $(3.74 \pm 0.31) \times 10^{-15}$  at/at) (Merchel et al., 2021). The purification of the samples largely followed the method  
183 outlined by Simon et al. (2016). The samples were evaporated, dissolved in distilled HCl and  $\text{NH}_3$  was added for  
184 Be oxy-hydroxide precipitation from the solution at pH 8 - 9. The precipitate was recovered by centrifugation and  
185 then dissolved in 1 mL distilled 10.2 M HCl before loading onto a column filled with 15 mL Dowex<sup>®</sup> 1 x 8 (100-  
186 200 mesh) anion-exchange resin in order to remove Fe from the sample. Prior, the resin was rinsed with 20 mL  
187 MilliQ<sup>®</sup> water and conditioned with 30 mL 10.2 M HCl. The sample was then loaded onto the column and eluted  
188 using 30 mL 10.2 M HCl. A column filled with 10 mL 50 x 8 (100 - 200 mesh) cation-exchange resin was used to  
189 separate Be from B and Al. The resin was treated with 20 mL MilliQ<sup>®</sup> water followed by 20 mL 1 M HCl. The  
190 sample was loaded onto the column and the first 25 mL 1 M HCl eluent, which contain mainly B, were discarded.  
191 Be was eluted and collected with the next addition of 90 mL 1 M HCl. The resulting Be oxy-hydroxides were  
192 precipitated at pH 8 - 9 by addition of  $\text{NH}_3$ , then separated by centrifugation and washed 3 times by rinsing with  
193 MilliQ<sup>®</sup> water to remove all chlorides. The purified Be oxy-hydroxides were transferred into quartz vials, dried  
194 at 80 °C overnight and finally calcinated to BeO at 900 °C for 2 h. The BeO was mixed with Nb powder (Nb:BeO  
195 = 4 : 1 by weight) and pressed into a Cu cathode-holder for accelerator mass spectrometer (AMS) measurements.  
196 One blank and one replicate were measured with each batch of samples in order to assess reproducibility and  
197 background during the extraction procedure.

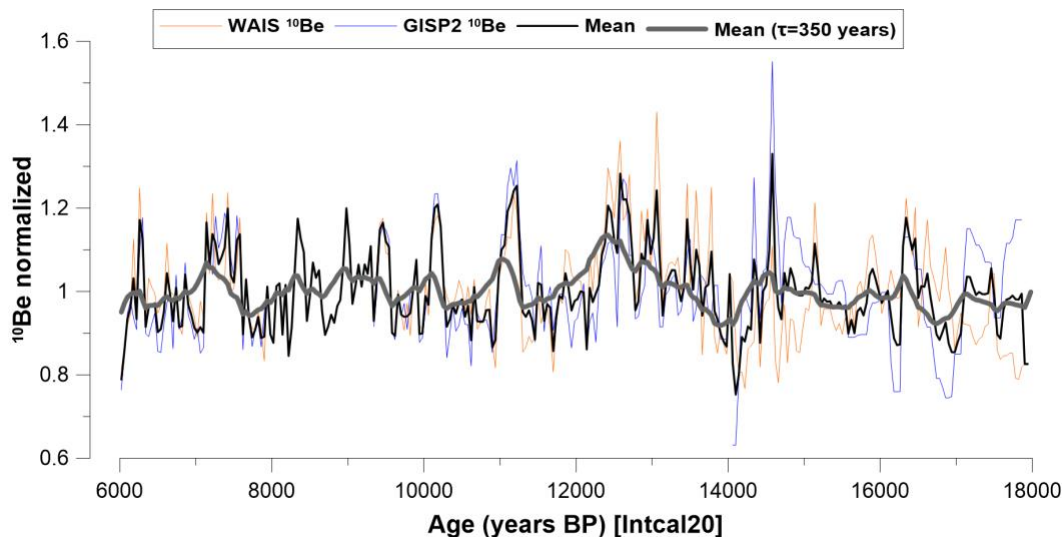
198 AMS measurements were performed at DREAMS (DREsden AMS) facility (Lachner et al., 2023; Rugel et al.,  
199 2016). All measurements were done relative to the standard “SMD-Be-12” with a weighted mean value of  $(1.704$   
200  $\pm 0.030) \times 10^{-12}$  (Akhmadaliev et al., 2013). Authigenic  $^{10}\text{Be}/^9\text{Be}$  was calculated from the AMS results, the known  
201 amount of carrier, and the measured authigenic  $^9\text{Be}$ -concentration from Inductively Coupled Plasma Atomic  
202 Emission Spectroscopy (ICP-AES) (see Simon et al., 2016). Considering the recent age of the samples, we did  
203 not correct for decay of  $^{10}\text{Be}$ . The correction would be in the order of 0.5 % and is an order of magnitude lower  
204 than our combined measurement precision.

205 The preparation and measurement of the 7 new benthic foraminifera samples were undertaken based on the  
206 standard operation procedures routinely used at the MICADAS  $^{14}\text{C}$  laboratory facility of the Alfred Wegener  
207 Institute (Mollenhauer et al., 2021). Prior to measurement, care was taken to critically select appropriate and  
208 sufficient number of foraminifera shells without brownish discolouration or authigenic calcite overgrowth to  
209 reduce uncertainty in the radiocarbon dates (Wollenburg et al., 2023).

#### 210 **2.4 Ice core $^{10}\text{Be}$ record**

211 The ice core  $^{10}\text{Be}$  record used in this study (Fig. 2) consists of normalized, averaged values of two ice cores: the  
212 West Antarctic Ice Sheet (WAIS) Divide ice core  $^{10}\text{Be}$  (Muschitiello et al., 2019; Sigl et al., 2016; Sinnl et al.,  
213 2023) and the Greenland Ice Sheet Project Two (GISP2)  $^{10}\text{Be}$  fluxes (Finkel and Nishiizumi, 1997). The ice core  
214 fluxes had been corrected for climate influences by performing a regression against  $\delta^{18}\text{O}$  and snow accumulation

215 rates (Adolphi et al., 2018). Prior to averaging, each ice core had been transferred to the IntCal20 timescale using  
 216 the timescale transfer functions described in several previous studies (Adolphi and Muscheler, 2016; Adolphi et  
 217 al., 2018 and Sigl et al., 2016). The glacial section of WAIS had been synchronized to Greenland Ice-Core  
 218 Chronology 2005 (GICC05) by using volcanic (Svensson et al., 2020) and cosmogenic (Sinnl et al., 2023) tie  
 219 points. The data from each ice core were resampled (averaged) to 40-year resolution before stacking. In order to  
 220 facilitate a comparison between ice core and marine  $^{10}\text{Be}$  changes, we modelled the expected marine signal from  
 221 the ice core record following Christl (2007). We chose a 350-year residence time of Beryllium in the water column  
 222 prior to deposition as this leads to a good agreement of amplitudes of the modelled centennial changes in  $^{10}\text{Be}$  to  
 223 the measured  $^{10}\text{Be}/^9\text{Be}$  changes seen in the sediment. This 350-year residence time is within the range of values  
 224 ( $80 \pm 5$  to  $500 \pm 25$  years) reported in Arctic Ocean calculated from sedimentary fluxes and inventories (Frank et  
 225 al., 2009).  
 226  
 227



228  
 229 **Figure 2: WAIS (orange)** (Muschitiello et al., 2019; Sigl et al., 2016; Sinnl et al., 2023) **and GISP2 (blue)** (Finkel and  
 230 Nishiizumi, 1997)  $^{10}\text{Be}$  fluxes corrected for correlation to ice core accumulation rates and  $\delta^{18}\text{O}$ , plotted on the IntCal20  
 231 timescale. The thick black line shows the mean of both datasets and the bold grey line depicts the modelled oceanic  $^{10}\text{Be}$   
 232 signal assuming a residence time ( $\tau$ ) of 350 years for  $^{10}\text{Be}$  in the water column.

233  
 234 **3 Results**

235 The concentrations of  $^9\text{Be}$ ,  $^{10}\text{Be}$  and  $^{10}\text{Be}/^9\text{Be}$  atomic ratios from core PS2458-4 are displayed in Fig. 3 and the  
 236 data are shown in Table S2. Five replicate samples of  $^{10}\text{Be}/^9\text{Be}$  ratios are shown in Table S3. The agreement  
 237 between these replicate measurements was assessed using the Coefficient of Variation (CV) for each depth. We  
 238 observe that the authigenic  $^{10}\text{Be}/^9\text{Be}$  ratios demonstrated relatively low CV values, ranging from 0.98% to 7.11%,  
 239 which is in agreement with the stated uncertainties of the  $^{10}\text{Be}/^9\text{Be}$ -ratio (Table S3). The dominant feature is an  
 240 increasing trend of  $^{10}\text{Be}/^9\text{Be}$  from the bottom to the top of the core. The modern surface sediment  $^{10}\text{Be}/^9\text{Be}$  values  
 241 ( $[0.54 - 0.76] \times 10^{-8}$ ) from the offshore transect spanning from the Lena Delta to the core site (Table 1, Fig. 1) are  
 242 consistent with  $^{10}\text{Be}/^9\text{Be}$  of Lena water samples ( $[0.62 \pm 0.07] \times 10^{-8}$ ) (Frank et al., 2009) and within the same  
 243 range as PS2458-4  $^{10}\text{Be}/^9\text{Be}$  ( $[0.53 - 1.77] \times 10^{-8}$ ). They show an increasing trend from the Lena Delta to the open

244 ocean (Fig. 1). The modern values close to the Lena are consistent with the lowest  $^{10}\text{Be}/^9\text{Be}$  values of PS2458-4  
 245 during the deglaciation, when the core-site was proximal to the paleo-river mouth of the Lena (see Figure 1).

246 **Table 1. Information about location, water depth, distance from Lena Delta and concentration of**  
 247 **authigenic  $^{10}\text{Be}$ ,  $^9\text{Be}$ ,  $^{10}\text{Be}/^9\text{Be}$  ratio leached of the modern surface sediment samples.**

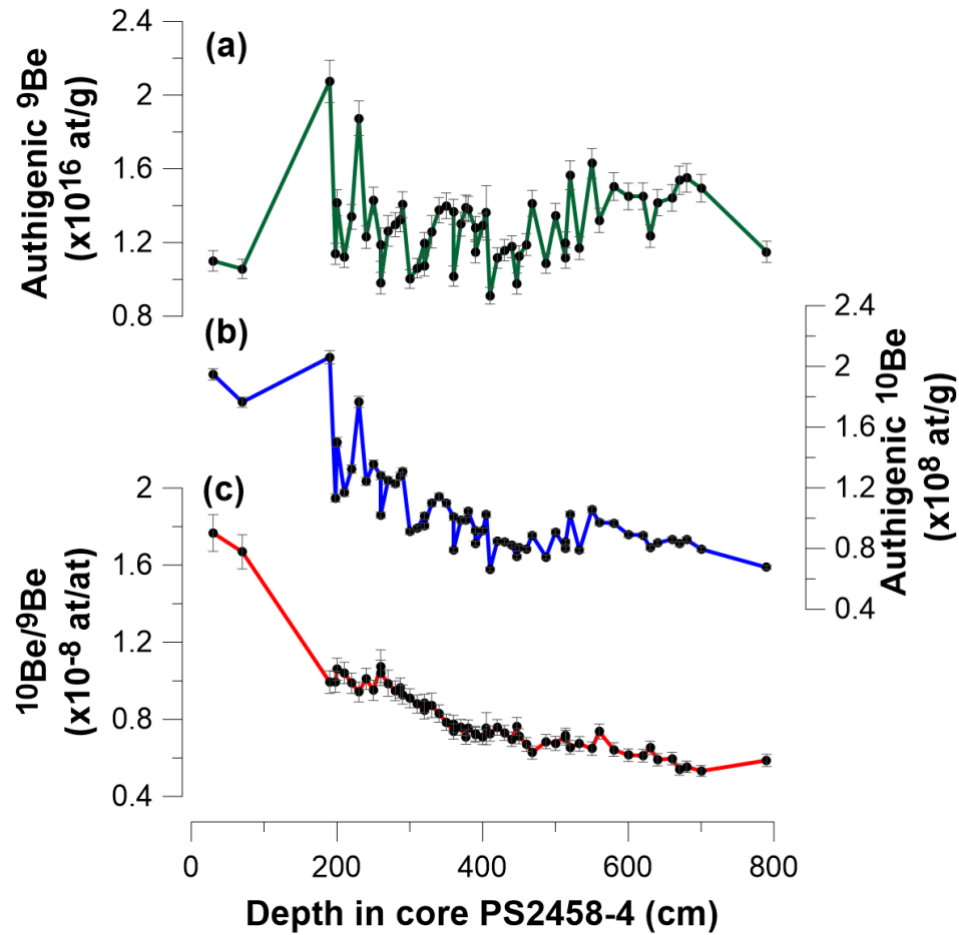
Sample name	Sample ID	Latitude (°)	Longitude (°)	Water Depth (m)	Approx. distance from Lena Delta (km)	$^9\text{Be}$ (at/g) [ $\times 10^{16}$ ]	$^{10}\text{Be}$ (at/g) [ $\times 10^8$ ]	$^{10}\text{Be}/^9\text{Be}$ (at/at) [ $\times 10^{-8}$ ]
IK93Z4-4	1	72.03	130.13	14	28	1.12	0.63	0.56
IK9307-3	2	72.55	131.30	20.7	61	1.60	0.86	0.54
IK9316-6	3	73.00	131.50	27.8	65	1.89	1.15	0.61
IK9318-5	4	73.50	137.55	24	269	1.58	0.92	0.59
IK9350-6	5	75.02	136.03	31	295	1.13	0.82	0.72
IK9373A-6	6	75.81	134.58	46	322	1.46	0.93	0.64
PS2728-2a-1	7	77.25	135.01	44	471	1.42	1.09	0.76
PS2458-4*	8	78.17	133.38	983	518	1.28	1.95	1.77

\*For core PS2458-4, the  $^9\text{B}$ ,  $^{10}\text{Be}$  and  $^{10}\text{Be}/^9\text{Be}$  results from the 30 cm sample are used as the core-top values.

248  
 249 In order to use  $^{10}\text{Be}/^9\text{Be}$  as a synchronization tool, we must remove this influence of mixing riverine and marine  
 250 endmembers. It is non-trivial to derive a quantitative end-member mixing model solely from local sea-level  
 251 reconstructions because sea-level only provides conceptual evidence about the variable proportions of open ocean  
 252 and riverine water masses bathing the core site. Hence, we chose a statistical model, assuming that the changes in  
 253 the endmember-mixing were gradual and hence, can be removed by normalizing to the long-term trend in the  
 254  $^{10}\text{Be}/^9\text{Be}$  record. The residual centennial variability in  $^{10}\text{Be}/^9\text{Be}$  is hypothesized to be driven by  $^{10}\text{Be}$ -production  
 255 rate changes and therefore suitable for synchronization.  
 256



257 Three different statistical models were used to test the sensitivity of our results to the choice of detrending  
 258 techniques. Figure 4a illustrates the three different trend fitting techniques (logarithmic, power, and LOESS  
 259 (LOcally Estimated Scatterplot Smoothing) applied to the  $^{10}\text{Be}/^9\text{Be}$  data set. The relative  $^{10}\text{Be}/^9\text{Be}$  residuals are  
 260 plotted with respect to the logarithmic, power and LOESS trends (Fig. 4b) and the differences fall within the  
 261 measurement uncertainties of the individual data points, showing that variations of the  $^{10}\text{Be}/^9\text{Be}$  ratio are robust  
 262 against the choice of the detrending model.



263

264 **Figure 3: Concentrations of (a)  $^9\text{Be}$ , (b)  $^{10}\text{Be}$  and (c)  $^{10}\text{Be}/^9\text{Be}$  atomic ratios from core PS2458-4**

265

266

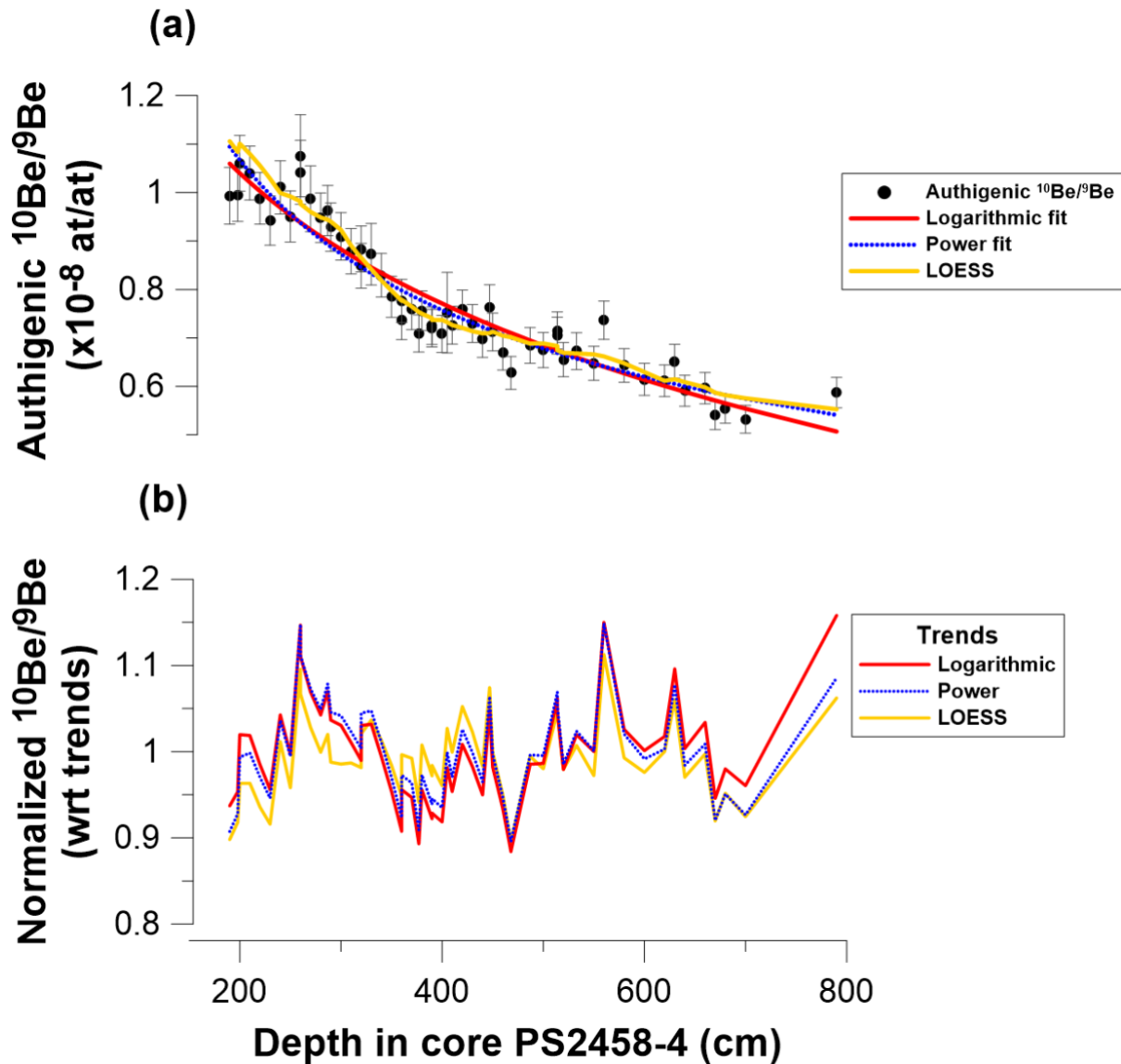


Figure 4: Sensitivity tests (a) Three different trend fitting techniques (logarithmic, power, and LOESS), (b) Relative  $^{10}\text{Be}/^9\text{Be}$  residuals with respect to logarithmic, power and LOESS trends

267  
268

269  
270

271

272 To check whether the detrended  $^{10}\text{Be}/^9\text{Be}$  record is driven by cosmogenic  $^{10}\text{Be}$  production rate changes, we  
 273 compare the detrended signal to the ice core  $^{10}\text{Be}$ -record. Figure 5 shows the ice core  $^{10}\text{Be}$  record and PS2458-4  
 274 mean profile of the three detrended data sets with a 3-point LOESS graph plotted on an initial  $^{14}\text{C}$ -based age-scale  
 275 (see used  $\Delta R$  value below). Note however, that the following analyses have been performed on all three versions  
 276 of the detrended dataset in order to test the robustness of our results against the choice of the detrending method.  
 277 The variations observed in the sediment  $^{10}\text{Be}/^9\text{Be}$  record follow closely the same pattern and relative amplitudes  
 278 compared with the ice core  $^{10}\text{Be}$  record. Therefore, we suggest that the variations observed in the  $^{10}\text{Be}/^9\text{Be}$  record  
 279 indeed reflect the production rate changes in the centennial range.

280

281 In order to refine the initial  $^{14}\text{C}$ -based chronology and infer a regional deglacial  $\Delta R$ -estimate, we constructed  $^{14}\text{C}$ -  
 282 based age-depth-models for PS2458-4 using OxCal 4.4 (Ramsey, 2009) assuming a range of  $\Delta R$  between -110

283 (Bauch et al., 2001) and +800 <sup>14</sup>C years. Each age-model was then evaluated by comparing the resulting PS2458-  
 284 4 <sup>10</sup>Be/<sup>9</sup>Be-timeseries to the ice core <sup>10</sup>Be-record. For this purpose, we use the generalized likelihood function by  
 285 Christen and Pérez, (2009) that is otherwise used for the calibration of <sup>14</sup>C-dates:

286

$$287 \quad L_{\Delta R} \propto \prod_{j=1}^n \left[ b + \frac{(x_j - y(t_j))^2}{2(\sigma_x^2 + \sigma_y^2)} \right]^{-(a+\frac{1}{2})}$$

288

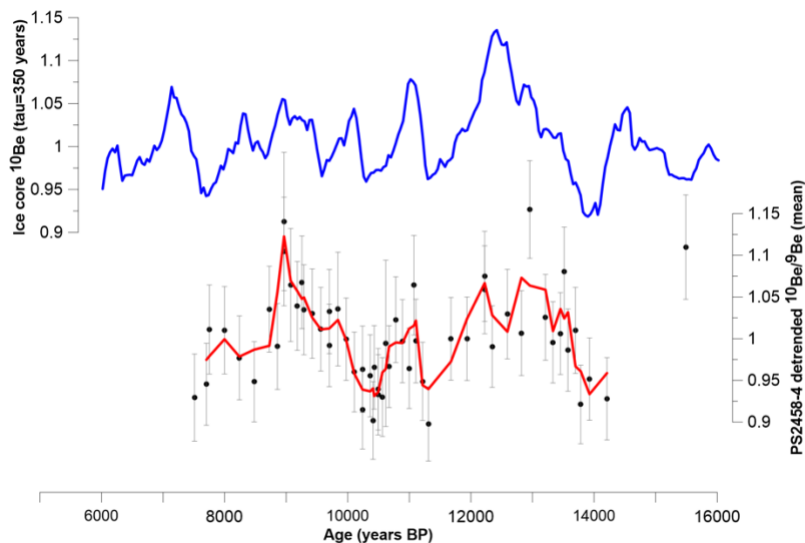
289 In our case, the ice core provides the calibration that describes <sup>10</sup>Be-anomalies at each point in time (y(t)) which  
 290 is compared to the sediment <sup>10</sup>Be/<sup>9</sup>Be (x<sub>j</sub>) on their modelled absolute age assuming a certain reservoir age. We use  
 291 a = 3 and b = 4 based on the recommendation of Christen and Pérez (2009). This allows us to use <sup>10</sup>Be to compare  
 292 the likelihoods of different age models, and thus <sup>14</sup>C-reservoir ages.

293

294 The likelihood values were calculated for each of the three different trend fitting techniques and are shown in  
 295 Figure 6. They result in a mean ΔR ± 1σ of 360 ± 75, 340 ± 50 and 335 ± 55 <sup>14</sup>C years for the logarithmic, power  
 296 and LOESS trend fitting techniques, respectively. These values are statistically indistinguishable and hence, we  
 297 opt for the arithmetic mean ΔR value of 345 ± 60 <sup>14</sup>C years. By using a global average marine reservoir age of  
 298 503 ± 63 <sup>14</sup>C years for the period 7.51-14.21 kyr BP (Heaton et al., 2020), we estimated a local MRA of 848 ± 90  
 299 <sup>14</sup>C years for the Laptev Sea during the deglaciation. The age-depth model for core PS2458-4 was reconstructed  
 300 using radiocarbon dates of mixed benthic bivalves and benthic foraminifera (Spielhagen et al., 2005). Therefore,  
 301 our calculated ΔR and corresponding MRA reflects to a benthic value.

302

303 The depositional age-depth model with a ΔR value of 345 ± 60 <sup>14</sup>C years for core PS2458-4 is shown in Figure  
 304 S2 in the Supplement accompanying this manuscript. Compared to the mean modelled ages calculated with a ΔR  
 305 value of -110 ± 28 <sup>14</sup>C years, the new modelled ages computed with a ΔR value of 345 ± 60 <sup>14</sup>C years were  
 306 observed to shift younger in the range of 429 to 707 years (Table S1).



307

308 **Figure 5: Ice core <sup>10</sup>Be record with tau=350 years (blue) and PS2458-4 record calculated from the mean of the three**  
 309 **detrended data sets with a 3-point LOESS graph using ΔR value of 345±60 <sup>14</sup>C years for age-model (red)**

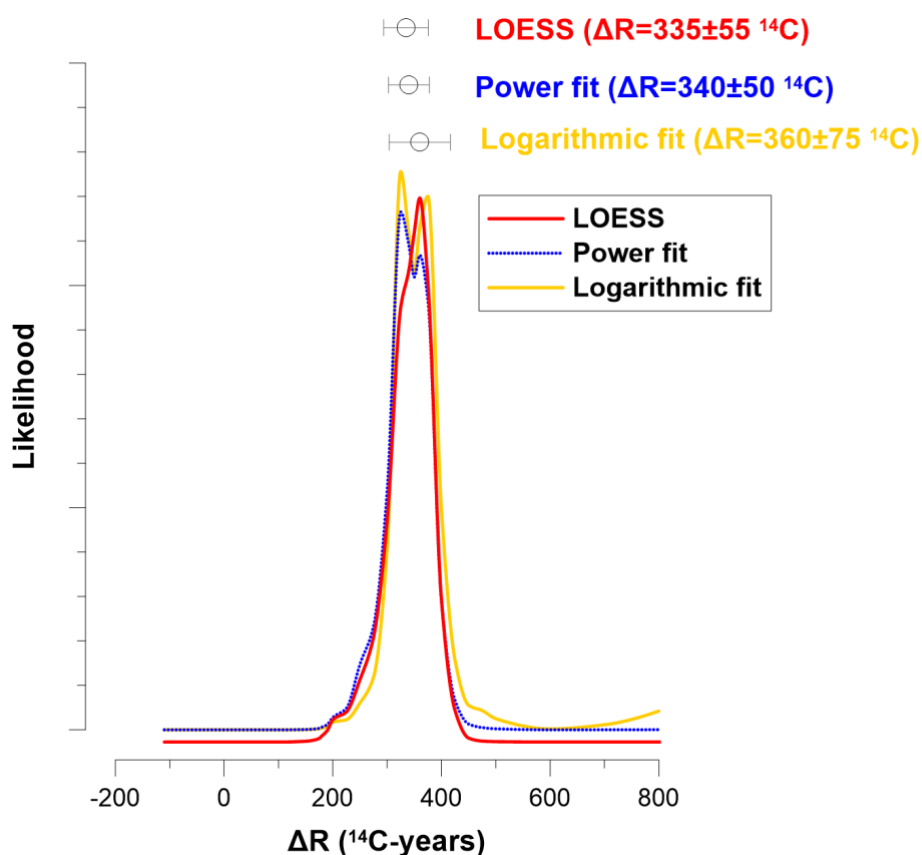
311  
312  
313  
314

Figure 6: Likelihood results with mean  $\Delta R \pm 1\sigma$  values of  $360 \pm 75$ ,  $340 \pm 50$  and  $335 \pm 55$   $^{14}\text{C}$  years BP based on LOESS (red), power (blue dotted) and logarithmic (yellow) trend fitting techniques respectively.

315

Table 2. Radiocarbon and modelled ages from foraminifera and bivalve samples from core PS2458-4

Depth (cm)	Sample ID	$^{14}\text{C}$ Age ( $^{14}\text{C}$ years)	$\pm$ (years)	Modelled Age (mean) (cal BP)	Modelled Age (cal BP, $2\sigma$ )	Sample type
667	KIA6113	12600	110	13745	14089 – 13360	mb, mbf
578	AAR-3087	12270	65	13198	13428 – 12982	mb
530	AAR-3086	11560	100	12551	12815 – 12244	mb
491*	AWI-7415.1.1	10968	159	11753	12220 – 11280	mbf
467	AAR-3085	10600	75	11291	11630 – 11005	mb
399	AAR-3084	10090	65	10551	10811 – 10276	mb
369	AAR-3083	10020	70	10357	10606 – 10135	mb
331.5*	AWI-7412.1.1	9596	122	9860	10183 – 9527	mbf
291.5*	AWI-7411.1.1	9089	224	9305	9711 – 8917	mbf
252	AAR-3082	8830	55	8880	9129 – 8615	mb
241.5*	AWI-7410.1.1	8762	141	8762	9058 – 8448	mbf
141.5*	AWI-7409.1.1	6447	158	6334	6696 – 5969	mbf
121.5*	AWI-7408.1.1	6029	134	5985	6297 – 5638	mbf
0.5*	AWI-7786.3.1	0		0		mbf

Modelled ages were calculated using OxCal4.4 (Ramsey, 2009) with a  $\Delta R$  value of  $345 \pm 60$   $^{14}\text{C}$  years BP, as calculated in this study. Marine  $^{14}\text{C}$  dates were calibrated with the Marine20 curve (Heaton et al., 2020). The depth values with asterisks represent the new benthic foraminifera samples measured for  $^{14}\text{C}$  dates. The depth values without asterisks show the  $^{14}\text{C}$  dates published  $^{14}\text{C}$  dates from Spielhagen et al. (2005). Libby half-life (5568 years) was used to calculate  $^{14}\text{C}$  age of foraminifera samples. Sample type: mb= mixed bivalves, mbf= mixed benthic foraminifera.

316

317

#### 318 4 Discussion

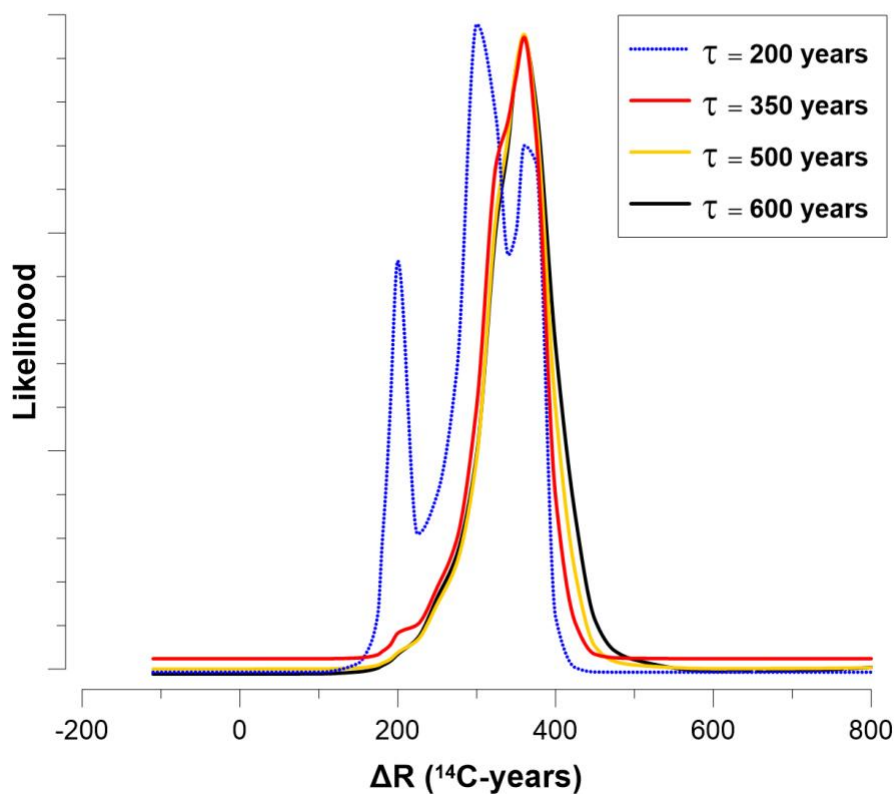
319 We have been able to quantitatively compare the agreement between ice core  $^{10}\text{Be}$  and sediment  $^{10}\text{Be}/^9\text{Be}$  for  
320 different  $\Delta R$  values and visually, we can observe how the two records representing cosmogenic radionuclide  
321 production variations are in-phase with each other. It is a more robust approach to compare whole timeseries by  
322 using a statistical method such as the likelihood function, instead of matching single wiggles or shorter time  
323 periods with each other from both records. The latter method is more prone to noise in each dataset and  
324 complicates the correct identification of matching peaks. By using just one single  $\Delta R$  value of  $345 \pm 60$   $^{14}\text{C}$  years,  
325 we found that there is a strong agreement between both the ice core  $^{10}\text{Be}$  and the sediment  $^{10}\text{Be}/^9\text{Be}$  records. This  
326 indirectly supports our constant  $\Delta R$  assumption, which implies a constant offset from Marine20 rather than a  
327 constant MRA (i.e., offset from IntCal20) throughout the studied period. Figure S2 illustrates the  $^{14}\text{C}$  ages of  
328 foraminifera samples plotted alongside with IntCal20 and Marine20 calibration curves. Figure S3 shows the non-  
329 polar global-average MRA corresponding to Marine20 and the inferred MRA, calculated as the difference between  
330 the atmospheric  $^{14}\text{C}$  age (derived from IntCal20) and the  $^{14}\text{C}$  age of foraminifera and bivalve samples. The inferred  
331 MRA data points demonstrate close alignment with the Marine20 MRA+ $\Delta R$  data, indicating a robust correlation.  
332 While this alignment is partially anticipated due to calibration with a constant  $\Delta R$ , the agreement between the  $^{14}\text{C}$ -  
333 based age model and  $^{10}\text{Be}$  data from ice core and sediment hence indicates that a time-variable  $\Delta R$  is not required  
334 to bring the  $^{10}\text{Be}$ -records in agreement.

335  
336 When modelling the ice core data, we have assumed a 350-year residence time of  $^{10}\text{Be}$  in the water column prior  
337 to deposition. We tested the influence of choosing different residence times of  $^{10}\text{Be}$  in the water column when  
338 modelling the ice core data and then synchronizing the modeled data sets with the PS2458-4  $^{10}\text{Be}/^9\text{Be}$ -timeseries.  
339 Different tau values ( $\tau = 200, 500, 600$  years) were used to model the ice core data and the  $\Delta R$ -likelihood values  
340 from the LOESS-smoothed  $^{10}\text{Be}$  record were calculated. We observed that for all assumed tau-values likelihood  
341 peaks occur at a  $\Delta R$  value of 360  $^{14}\text{C}$  years (Fig. 7). This indicates that the most likely  $\Delta R$  value is not strongly  
342 dependent on the different assumed tau values. We found that only for the tau value of 200 years another best  
343 likelihood estimate occurs at a  $\Delta R$  value of 300  $^{14}\text{C}$  years BP, followed by the secondary likelihood maximum at  
344 a  $\Delta R$  value of 360  $^{14}\text{C}$  years BP. Figure S4 shows the modelled ice core time series with a tau value of 200 years,  
345 which indicates clearly larger  $^{10}\text{Be}$  amplitudes than what was calculated with a tau value of 350 years, which are  
346 larger than the  $^{10}\text{Be}/^9\text{Be}$  changes seen in PS2458-4. Based on these results, it seems unlikely that the best likelihood  
347 estimate occurring at a  $\Delta R$  value of 300  $^{14}\text{C}$  years BP with tau=200 years is real.

348  
349 Our calculated local benthic MRA value of  $848 \pm 90$   $^{14}\text{C}$  years BP is consistent with the modern values calculated  
350 by Bauch et al. (2001), which range from  $295 \pm 45$  to  $860 \pm 55$   $^{14}\text{C}$  years. The largest modern reservoir age of  $860$   
351  $\pm 55$   $^{14}\text{C}$  years is located closest to the Lena Delta, which is comparable to the setting of the location of core  
352 PS2458-4 during deglaciation around 14 - 12 kyr BP. Another study from the central Arctic Ocean reported MRA  
353 values of 1400  $^{14}\text{C}$  years BP ( $\Delta R = 1000$ ) during the Late Glacial and 700  $^{14}\text{C}$  years BP ( $\Delta R = 300$ ) during the  
354 Holocene (Hanslik et al., 2010).

355  
356 The  $\Delta R$  value was calculated during the deglaciation (14-8 kyr BP) and during this period the mean relative sea  
357 level rose by about 64 m (Klemann et al., 2015). The core was retrieved at a depth of 983 m in 1994 and at 14 and

358 8 kyr BP the depths were about 903 and 967 m respectively. Moreover, as shown in Figure 1, the modern surface  
 359  $^{10}\text{Be}/^9\text{Be}$  values show an increasing trend from the Lena Delta to the open ocean (Fig. 1). Thus, we attribute the  
 360 trend in PS2458-4  $^{10}\text{Be}/^9\text{Be}$  to deglacial sea level rise and the associated coastline retreat (Bauch et al., 2001;  
 361 Klemann et al., 2015). During the glacial period, the core site was located close to the Lena River mouth and  
 362 hence, bathed in river-water with low  $^{10}\text{Be}/^9\text{Be}$ . With increasing sea-level and coastline retreat, open ocean waters  
 363 with higher  $^{10}\text{Be}/^9\text{Be}$  became more dominant.



364  
 365 **Figure 7. Likelihood results based on different  $\Delta R$  for the LOESS-smoothed ice core  $^{10}\text{Be}$  using for different tau values**  
 366 **of 200, 350, 500 and 600 years.**

367  
 368 We compared our estimated  $\Delta R$  value  $345 \pm 60$   $^{14}\text{C}$  years with the approach proposed by Heaton et al. (2023) to  
 369 infer glacial  $\Delta R$  values in polar regions. In the polar regions (outside  $40^\circ \text{S} - 40^\circ \text{N}$ ), it is expected that during  
 370 glacial episodes, there may have been regional differences in the amount of oceanic  $^{14}\text{C}$  depletion compared to  
 371 the global non-polar ocean mean represented by Marine20. The increase in the volume and density of sea ice  
 372 limiting air-sea gas-exchange may cause a significant larger  $\Delta R$  during the glacial era compared to the interglacial  
 373 values. For glacial periods (55.0 - 11.5 kyr BP), Heaton et al. (2023) proposed a latitude-dependent method to  
 374 infer upper bounds of the possible  $\Delta R$  difference between Holocene and Glacial in polar regions. A lower bound  
 375  $\Delta R^{\text{Hol}}$  is based on samples from the Holocene and an upper (glacial) bound  $\Delta R^{\text{GS}}$ , is calculated by increasing  $\Delta R^{\text{Hol}}$   
 376 depending on the latitude.

377

378 The PS2458-4 record used in this study extends from about 7.5 to 14.2 kyr BP and therefore covers the early  
379 Holocene and parts of the deglacial period. Thus, from 11.5 to 14.2 kyr BP, the record extends into the glacial and  
380 samples from this period may require a glacial polar boost as proposed by Heaton et al. (2023). We calculated  
381  $\Delta R^{\text{Hol}}$  from  $^{14}\text{C}$  samples found in the online database at <http://calib.org/marine/> (Reimer and Reimer, 2001). Using  
382 the weighed mean value of the 5 nearest  $\Delta R$  values from the core location in the Laptev Sea from Bauch et al.  
383 (2001), yields a  $\Delta R^{\text{Hol}}$  value of  $-95 \pm 61$   $^{14}\text{C}$  years.  $\Delta R^{\text{GS}}$  was calculated as:  $\Delta R^{\text{GS}} = \Delta R^{\text{Hol}} + \Delta R^{\text{Hol} \rightarrow \text{GS}}$ , in agreement  
384 with the GS scenario as described in Heaton et al. (2023). The value  $\Delta R^{\text{Hol} \rightarrow \text{GS}}$  is dependent on the latitude of the  
385 sample and at  $78.75^\circ\text{N}$ , it amounts to 790  $^{14}\text{C}$  years. The resulting  $\Delta R^{\text{GS}}$  value is  $695 \pm 61$   $^{14}\text{C}$  years and is much  
386 larger than our inferred benthic  $\Delta R$  value ( $345 \pm 60$   $^{14}\text{C}$  years).

387  
388 These differences are likely due to distinct regional changes in climate and hydrology. At the core location in the  
389 Laptev Sea, sea-ice cover was less during the Younger Dryas and Heinrich Stadial 1 compared to the Holocene  
390 (Fahl and Stein, 2012), contrary to large-scale deglacial sea ice trends included in the model by Heaton et al.  
391 (2023). The expansion of regional sea-ice cover during the recent past in the Laptev Sea could have further  
392 influenced the  $\Delta R$  value, which then should have been larger during the Holocene compared to the early  
393 deglaciation. However, our calculated  $\Delta R$  value of  $345 \pm 60$   $^{14}\text{C}$  years is larger than the modern average  $\Delta R$  value  
394 of  $-95 \pm 61$   $^{14}\text{C}$  years, making it unlikely that sea-ice cover dynamics were the main driver of past changes in  
395 regional  $\Delta R$ . Instead, as mentioned before, the local reservoir ages in the region are spatially highly variable and  
396 influenced by a hardwater effect (Bauch et al. 2001). These regional processes are thus site specific and hence,  
397 obviously cannot be covered by the approach of Heaton et al. (2023). Bauch et al. (2001) reported that the  
398 relatively old  $^{14}\text{C}$ -age of bivalve shells collected in proximity of the Lena Delta near Tiksi Bay, might be due to  
399 the influence of local hardwater effect. This is consistent with the modern setting where the largest  $\Delta R$  is found  
400 close to the Lena Delta and lower  $\Delta R$  towards the shelf-edge (Bauch et al., 2001). Hence, the larger deglacial  $\Delta R$   
401 of PS2458-4 could be driven by its proximity to the Lena River during that time as evidenced by low  $^{10}\text{Be}/^9\text{Be}$  as  
402 discussed earlier.

403  
404

## 405 **5 Conclusion**

406 We present high-resolution  $^9\text{Be}$  and  $^{10}\text{Be}$  records reconstructed from core PS2458-4, which was retrieved from the  
407 continental slope of the eastern Laptev Sea in the Arctic Ocean. We demonstrate that these records are influenced  
408 by the distance of the core site to the Lena River, which changed depending on sea-level. Centennial to millennial  
409 scale variability in the  $^{10}\text{Be}/^9\text{Be}$  ratio can be attributed to variations in production rate and can hence be used to  
410 correlate our sediment record to ice-core  $^{10}\text{Be}$  records.

411  
412 This is the first study to reconstruct high-resolution  $^{10}\text{Be}$  production rate changes from  $^{10}\text{Be}/^9\text{Be}$  records from  
413 Arctic marine sediments for correlation to ice cores, and this approach has been applied with success. We have  
414 correlated the  $^{10}\text{Be}$  from marine sediment core PS2458-4 with  $^{10}\text{Be}$  from ice core and used a likelihood function  
415 to estimate  $\Delta R$  values.

416

417 Our estimate for the deglacial benthic  $\Delta R$  value for the Laptev Sea is  $345 \pm 60$   $^{14}\text{C}$  years BP corresponding to a  
418 MRA of  $848 \pm 90$   $^{14}\text{C}$  years. The  $\Delta R$  value will be used to refine the age-depth model for core PS2458-4 from the  
419 Laptev Sea, which could be used as a reference chronology for the Laptev Sea.

420

#### 421 **Data availability**

422

423 The  $^9\text{Be}$ ,  $^{10}\text{Be}$  and  $^{10}\text{Be}/^9\text{Be}$  data sets from core PS2458-4 generated in this study are available as a Supplement  
424 to this paper.

425

#### 426 **Author contributions**

427

428 FA and GM designed the study. AN, MM conducted the laboratory analyses and FA, AN and GM analyzed the  
429 data. JL and KS were responsible for preparation and conduction of the  $^{10}\text{Be}$  AMS measurements. JW selected  
430 appropriate foraminifera samples for radiocarbon dating. HG undertook the radiocarbon measurement of the  
431 foraminifera samples and analyzed the data. AN drafted a first version of the paper and FA and AN generated the  
432 figures. All co-authors contributed to the writing and provided feedback on the paper.

433

#### 434 **Competing interests**

435

436 The contact author has declared that neither of the authors has any competing interests.

437

438

#### 439 **Acknowledgements**

440

441 Parts of this research were carried out at the Ion Beam Centre (IBC) at the Helmholtz-Zentrum Dresden-  
442 Rossendorf e. V., a member of the Helmholtz Association. We would like to thank the DREAMS operator team  
443 for their assistance with AMS-measurements. FA was supported by the Helmholtz Association (VH-NG 1501).  
444 We are grateful for the technical support offered by Torben Gentz and Elizabeth Bonk from the MICADAS facility  
445 at AWI Bremerhaven. AN would like to thank DAAD and POLMAR for support during his doctoral studies.

446

447

448

449

450

451

452

453

454

455

456

457

458

459

460

461

462

463

464



465 **References**

- 466 Adolphi, F. and Muscheler, R.: Synchronizing the Greenland ice core and radiocarbon timescales over the  
467 Holocene-Bayesian wiggle-matching of cosmogenic radionuclide records, *Climate of the Past*, 12, 15–30,  
468 <https://doi.org/10.5194/cp-12-15-2016>, 2016.
- 469 Adolphi, F., Bronk Ramsey, C., Erhardt, T., Edwards, R. L., Cheng, H., Turney, C. S. M., Cooper, A., Svensson, A.,  
470 Rasmussen, S. O., Fischer, H., and Muscheler, R.: Connecting the Greenland ice-core and U/Th timescales via  
471 cosmogenic radionuclides: testing the synchronicity of Dansgaard–Oeschger events, *Climate of the Past*, 14,  
472 1755–1781, <https://doi.org/10.5194/cp-14-1755-2018>, 2018.
- 473 Adolphi, F., Herbst, K., Nilsson, A., and Panovska, S.: On the Polar Bias in Ice Core 10Be Data, *Journal of*  
474 *Geophysical Research: Atmospheres*, 128, <https://doi.org/10.1029/2022JD038203>, 2023.
- 475 Akhmadaliev, S., Heller, R., Hanf, D., Rugel, G., and Merchel, S.: The new 6MV AMS-facility DREAMS at  
476 Dresden, *Nucl Instrum Methods Phys Res B*, 294, 5–10, <https://doi.org/10.1016/j.nimb.2012.01.053>, 2013.
- 477 Alves, E. Q., Macario, K., Ascough, P., and Bronk Ramsey, C.: The Worldwide Marine Radiocarbon Reservoir  
478 Effect: Definitions, Mechanisms, and Prospects, *Reviews of Geophysics*, 56, 278–305,  
479 <https://doi.org/https://doi.org/10.1002/2017RG000588>, 2018.
- 480 Audi, G., Bersillon, O., Blachot, J., and Wapstra, A. H.: The NUBASE evaluation of nuclear and decay properties,  
481 *Nucl Phys A*, 729, <https://doi.org/10.1016/j.nuclphysa.2003.11.001>, 2003.
- 482 Bauch, H. A., Mueller-Lupp, T., Taldenkova, E., Spielhagen, R. F., Kassens, H., Grootes, P. M., Thiede, J.,  
483 Heinemeier, J., and Petryashov, V. V.: Chronology of the holocene transgression at the north siberian margin,  
484 *Glob Planet Change*, 31, [https://doi.org/10.1016/S0921-8181\(01\)00116-3](https://doi.org/10.1016/S0921-8181(01)00116-3), 2001.
- 485 Von Blanckenburg, F. and Bouchez, J.: River fluxes to the sea from the ocean’s 10Be/9Be ratio, *Earth Planet Sci*  
486 *Lett*, 387, 34–43, <https://doi.org/10.1016/j.epsl.2013.11.004>, 2014.
- 487 von Blanckenburg, F., Bouchez, J., Ibarra, D. E., and Maher, K.: Stable runoff and weathering fluxes into the  
488 oceans over Quaternary climate cycles, *Nat Geosci*, 8, 538–542, <https://doi.org/10.1038/ngeo2452>, 2015.
- 489 Bourles, D., Raisbeck, G. M., and Yiou, F.: 10Be and 9Be in marine sediments and their potential for dating, 443–  
490 452 pp., 1989.
- 491 Chmeleff, J., von Blanckenburg, F., Kossert, K., and Jakob, D.: Determination of the 10Be half-life by  
492 multicollector ICP-MS and liquid scintillation counting, *Nucl Instrum Methods Phys Res B*, 268, 192–199,  
493 <https://doi.org/10.1016/j.nimb.2009.09.012>, 2010.
- 494 Christen, A. J. and Pérez, S. E.: A new robust statistical model for radiocarbon data, *Radiocarbon*, 51,  
495 <https://doi.org/10.1017/s003382220003410x>, 2009.
- 496 Christl, M.: Sensitivity and response of beryllium-10 in marine sediments to rapid production changes  
497 (geomagnetic events): A box model study, *Geochemistry, Geophysics, Geosystems*, 8,  
498 <https://doi.org/10.1029/2007GC001598>, 2007.
- 499 Czymzik, M., Dreibrodt, S., Feeser, I., Adolphi, F., and Brauer, A.: Mid-Holocene humid periods reconstructed  
500 from calcite varves of the Lake Woserin sediment record (north-eastern Germany), *Holocene*, 26, 935–946,  
501 <https://doi.org/10.1177/0959683615622549>, 2016a.
- 502 Czymzik, M., Muscheler, R., and Brauer, A.: Solar modulation of flood frequency in central Europe during spring  
503 and summer on interannual to multi-centennial timescales, *Climate of the Past*, 12, 799–805,  
504 <https://doi.org/10.5194/cp-12-799-2016>.
- 505 Czymzik, M., Muscheler, R., Adolphi, F., Mekhaldi, F., Dräger, N., Ott, F., Slowinski, M., Blaszkiewicz, M.,  
506 Aldahan, A., Possnert, G., and Brauer, A.: Synchronizing 10Be in two varved lake sediment records to IntCal13  
507 14C during three grand solar minima, *Climate of the Past*, 14, 687–696, <https://doi.org/10.5194/cp-14-687-2018>,  
508 2018.
- 509 Czymzik, M., Nowaczyk, N. R., Dellwig, O., Wegwerth, A., Muscheler, R., Christl, M., and Arz, H. W.: Lagged  
510 atmospheric circulation response in the Black Sea region to Greenland Interstadial 10,  
511 <https://doi.org/10.1073/pnas.2005520117/-/DCSupplemental>, 2020.
- 512 Dunai, T. J. and Lifton, N. A.: The nuts and bolts of cosmogenic nuclide production, *Elements*, 10, 347–350,  
513 <https://doi.org/10.2113/gselements.10.5.347>, 2014.
- 514 Fahl, K. and Stein, R.: Modern seasonal variability and deglacial/Holocene change of central Arctic Ocean sea-ice  
515 cover: New insights from biomarker proxy records, *Earth Planet Sci Lett*, 351–352, 123–133,  
516 <https://doi.org/10.1016/j.epsl.2012.07.009>, 2012.
- 517 Finkel, R. C. and Nishiizumi, K.: Beryllium 10 concentrations in the Greenland Ice Sheet Project 2 ice core from  
518 3-40 ka, *J Geophys Res Oceans*, 102, <https://doi.org/10.1029/97JC01282>, 1997.
- 519 Frank, M., Porcelli, D., Andersson, P., Baskaran, M., Björk, G., Kubik, P. W., Hattendorf, B., and Guenther, D.:  
520 The dissolved Beryllium isotope composition of the Arctic Ocean, *Geochim Cosmochim Acta*, 73,  
521 <https://doi.org/10.1016/j.gca.2009.07.010>, 2009.
- 522 Fütterer, D. K.: The expedition ARCTIC’93, Leg ARK-IX/4 of RV “Polarstern” 1993, Report on Polar Research,  
523 149, 244pp., 1994.

524 Gutjahr, M., Frank, M., Stirling, C. H., Klemm, V., van de Flierdt, T., and Halliday, A. N.: Reliable extraction of a  
525 deepwater trace metal isotope signal from Fe-Mn oxyhydroxide coatings of marine sediments, *Chem Geol*, 242,  
526 351–370, <https://doi.org/10.1016/j.chemgeo.2007.03.021>, 2007.

527 Hanslik, D., Jakobsson, M., Backman, J., Björck, S., Sellén, E., O’Regan, M., Fornaciari, E., and Skog, G.:  
528 Quaternary Arctic Ocean sea ice variations and radiocarbon reservoir age corrections, *Quat Sci Rev*, 29,  
529 <https://doi.org/10.1016/j.quascirev.2010.06.011>, 2010.

530 Heaton, T. J., Köhler, P., Butzin, M., Bard, E., Reimer, R. W., Austin, W. E. N., Bronk Ramsey, C., Grootes, P. M.,  
531 Hughen, K. A., Kromer, B., Reimer, P. J., Adkins, J., Burke, A., Cook, M. S., Olsen, J., and Skinner, L. C.:  
532 Marine20 - The Marine Radiocarbon Age Calibration Curve (0-55,000 cal BP), *Radiocarbon*, 62,  
533 <https://doi.org/10.1017/RDC.2020.68>, 2020.

534 Heaton, T. J., Butzin, M., Bard, E., Bronk Ramsey, C., Hughen, K. A., Kohler, P., and Reimer, P. J.: Marine  
535 radiocarbon calibration in polar regions: A simple approximate approach using marine20, *Radiocarbon*, 65,  
536 <https://doi.org/10.1017/RDC.2023.42>, 2023.

537 Heikkilä, U., Beer, J., Abreu, J. A., and Steinhilber, F.: On the atmospheric transport and deposition of the  
538 cosmogenic radionuclides ( $^{10}\text{Be}$ ): A review, <https://doi.org/10.1007/s11214-011-9838-0>, June 2013.

539 Kassens, H. and Dmitrenko, I.: Russian-German Cooperation: The TRANSDRIFT II expedition to the Laptev Sea.,  
540 *Reports on Polar Research*, 182, 1–180, 1995.

541 Kassens, H. and Karpiy, V. Y.: Russian-German cooperation: the transdrift I expedition to the Laptev sea., *Reports*  
542 *on Polar Research*, 151–168, 1994.

543 Klemann, V., Heim, B., Bauch, H. A., Wetterich, S., and Opel, T.: Sea-level evolution of the Laptev Sea and the  
544 East Siberian Sea since the last glacial maximum, *arXiv*, 1, <https://doi.org/10.1007/s41063-015-0004-x>, 2015.

545 Korschinek, G., Bergmaier, A., Faestermann, T., Gerstmann, U. C., Knie, K., Rugel, G., Wallner, A., Dillmann, I.,  
546 Dollinger, G., von Gostomski, C. L., Kossert, K., Maiti, M., Poutivtsev, M., and Remmert, A.: A new value for  
547 the half-life of  $^{10}\text{Be}$  by Heavy-Ion Elastic Recoil Detection and liquid scintillation counting, *Nucl Instrum*  
548 *Methods Phys Res B*, 268, 187–191, <https://doi.org/10.1016/j.nimb.2009.09.020>, 2010.

549 Lachner, J., Rugel, G., Vivo Vilches, C., Koll, D., Stübner, K., Winkler, S., and Wallner, A.: Optimization of  $^{10}\text{Be}$   
550 measurements at the 6 MV AMS facility DREAMS, *Nucl Instrum Methods Phys Res B*, 535, 29–33,  
551 <https://doi.org/10.1016/j.nimb.2022.11.008>, 2023.

552 Lal, D. and Peters, B.: Cosmic Ray Produced Radioactivity on the Earth. In: *Handbuch der Physik*, vol. XLVI/2.  
553 Springer, New York, 551–612 pp., 1967.

554 Masarik, J. and Beer, J.: Simulation of particle fluxes and cosmogenic nuclide production in the Earth’s  
555 atmosphere, *Journal of Geophysical Research Atmospheres*, 104, <https://doi.org/10.1029/1998JD200091>, 1999.

556 Merchel, S., Braucher, R., Lachner, J., and Rugel, G.: Which is the best  $^9\text{Be}$  carrier for  $^{10}\text{Be}/^9\text{Be}$  accelerator mass  
557 spectrometry?, *MethodsX*, 8, <https://doi.org/10.1016/j.mex.2021.101486>, 2021.

558 Mollenhauer, G., Grotheer, H., Gentz, T., Bonk, E., and Hefter, J.: Standard operation procedures and performance  
559 of the MICADAS radiocarbon laboratory at Alfred Wegener Institute (AWI), Germany, *Nucl Instrum Methods*  
560 *Phys Res B*, 496, <https://doi.org/10.1016/j.nimb.2021.03.016>, 2021.

561 Muscheler, R., Kromer, B., Björck, S., Svensson, A., Friedrich, M., Kaiser, K. F., and Southon, J.: Tree rings and  
562 ice cores reveal  $^{14}\text{C}$  calibration uncertainties during the Younger Dryas, *Nat Geosci*, 1,  
563 <https://doi.org/10.1038/ngeo128>, 2008.

564 Muscheler, R., Adolphi, F., and Knudsen, M. F.: Assessing the differences between the IntCal and Greenland ice-  
565 core time scales for the last 14,000 years via the common cosmogenic radionuclide variations, *Quat Sci Rev*,  
566 106, 81–87, <https://doi.org/10.1016/j.quascirev.2014.08.017>, 2014.

567 Muschitiello, F., D’Andrea, W. J., Schmittner, A., Heaton, T. J., Balascio, N. L., deRoberts, N., Caffee, M. W.,  
568 Woodruff, T. E., Welten, K. C., Skinner, L. C., Simon, M. H., and Dokken, T. M.: Deep-water circulation  
569 changes lead North Atlantic climate during deglaciation, *Nat Commun*, 10, <https://doi.org/10.1038/s41467-019-09237-3>, 2019.

571 Poluianov, S. V., Kovaltsov, G. A., Mishev, A. L., and Usoskin, I. G.: Production of cosmogenic isotopes  $^7\text{Be}$ ,  
572  $^{10}\text{Be}$ ,  $^{14}\text{C}$ ,  $^{22}\text{Na}$ , and  $^{36}\text{Cl}$  in the atmosphere: Altitudinal profiles of yield functions, *J Geophys Res*, 121,  
573 <https://doi.org/10.1002/2016JD025034>, 2016.

574 Rachor, E.: Scientific cruise report of the Arctic expedition ARK-XI/1 of RV “Polarstern” in 1995, *Reports on*  
575 *Polar and Marine Research*, 226, 1–336, 1997.

576 Raisbeck, G. M., Yiou, F., Fruneau, M., Loiseaux, J. M., Lieuvin, M., and Ravel, J. C.: Cosmogenic  $^{10}\text{Be}/^7\text{Be}$  as a  
577 probe of atmospheric transport processes, *Geophys Res Lett*, 8, 1015–1018,  
578 <https://doi.org/10.1029/GL008i009p01015>, 1981.

579 Ramsey, C. B.: Bayesian analysis of radiocarbon dates, *Radiocarbon*, 51,  
580 <https://doi.org/10.1017/s0033822200033865>, 2009.

581 Reimer, P. J. and Reimer, R. W.: A marine reservoir correction database and on-line interface, *Radiocarbon*, 43,  
582 <https://doi.org/10.1017/s0033822200038339>, 2001.

583 Reinig, F., Wacker, L., Jöris, O., Oppenheimer, C., Guidobaldi, G., Nievergelt, D., Adolphi, F., Cherubini, P.,  
 584 Engels, S., Esper, J., Land, A., Lane, C., Pfanz, H., Remmele, S., Sigl, M., Sookdeo, A., and Büntgen, U.:  
 585 Precise date for the Laacher See eruption synchronizes the Younger Dryas, *Nature*, 595,  
 586 <https://doi.org/10.1038/s41586-021-03608-x>, 2021.

587 Rugel, G., Pavetich, S., Akhmadaliev, S., Enamorado Baez, S. M., Scharf, A., Ziegenrucker, R., and Merchel, S.:  
 588 The first four years of the AMS-facility DREAMS: Status and developments for more accurate radionuclide  
 589 data, *Nucl Instrum Methods Phys Res B*, 370, 94–100, <https://doi.org/10.1016/j.nimb.2016.01.012>, 2016.

590 Schlitzer, R.: Ocean Data View, <https://odv.awi.de>, 2016.

591 Sigl, M., Fudge, T. J., Winstrup, M., Cole-Dai, J., Ferris, D., McConnell, J. R., Taylor, K. C., Welten, K. C.,  
 592 Woodruff, T. E., Adolphi, F., Bisiaux, M., Brook, E. J., Buizert, C., Caffee, M. W., Dunbar, N. W., Edwards, R.,  
 593 Geng, L., Iverson, N., Koffman, B., Layman, L., Maselli, O. J., McGwire, K., Muscheler, R., Nishiizumi, K.,  
 594 Pasteris, D. R., Rhodes, R. H., and Sowers, T. A.: The WAIS Divide deep ice core WD2014 chronology – Part 2:  
 595 Annual-layer counting (0–31 ka BP), *Climate of the Past*, 12, 769–786, <https://doi.org/10.5194/cp-12-769-2016>,  
 596 2016.

597 Simon, Q., Thouveny, N., Bourlès, D. L., Nuttin, L., Hillaire-Marcel, C., and St-Onge, G.: Authigenic  $^{10}\text{Be}/^{9}\text{Be}$   
 598 ratios and  $^{10}\text{Be}$ -fluxes ( $^{230}\text{Th}$ s-normalized) in central Baffin Bay sediments during the last glacial cycle:  
 599 Paleoenvironmental implications, *Quat Sci Rev*, 140, 142–162, <https://doi.org/10.1016/j.quascirev.2016.03.027>,  
 600 2016.

601 Sinnl, G., Adolphi, F., Christl, M., Welten, K. C., Woodruff, T., Caffee, M., Svensson, A., Muscheler, R., and  
 602 Rasmussen, S. O.: Synchronizing ice-core and U/Th timescales in the Last Glacial Maximum using Hulu Cave  
 603  $^{14}\text{C}$  and new  $^{10}\text{Be}$  measurements from Greenland and Antarctica, *Climate of the Past*, 19,  
 604 <https://doi.org/10.5194/cp-19-1153-2023>, 2023.

605 Southon, J.: A first step to reconciling the GRIP and GISP2 Ice-core chronologies, 0-14, 500 yr B.P., *Quat Res*, 57,  
 606 <https://doi.org/10.1006/qres.2001.2295>, 2002.

607 Spielhagen, R. F., Erlenkeuser, H., and Siebert, C.: History of freshwater runoff across the Laptev Sea (Arctic)  
 608 during the last deglaciation, *Glob Planet Change*, 48, 187–207, <https://doi.org/10.1016/j.gloplacha.2004.12.013>,  
 609 2005.

610 Stuiver, M., Pearson, G. W., and Braziunas, T.: Radiocarbon Age Calibration of Marine Samples Back to 9000 Cal  
 611 Yr BP, *Radiocarbon*, 28, <https://doi.org/10.1017/s0033822200060264>, 1986.

612 Svensson, A., Dahl-Jensen, D., Steffensen, J. P., Blunier, T., Rasmussen, S. O., Vinther, B. M., Vallelonga, P.,  
 613 Capron, E., Gkinis, V., Cook, E., Astrid Kjær, H., Muscheler, R., Kipfstuhl, S., Wilhelms, F., Stocker, T. F.,  
 614 Fischer, H., Adolphi, F., Erhardt, T., Sigl, M., Landais, A., Parrenin, F., Buizert, C., McConnell, J. R., Severi,  
 615 M., Mulvaney, R., and Bigler, M.: Bipolar volcanic synchronization of abrupt climate change in Greenland and  
 616 Antarctic ice cores during the last glacial period, *Climate of the Past*, 16, [https://doi.org/10.5194/cp-16-1565-](https://doi.org/10.5194/cp-16-1565-2020)  
 617 2020, 2020.

618 Wittmann, H., von Blanckenburg, F., Mohtadi, M., Christl, M., and Bernhardt, A.: The competition between coastal  
 619 trace metal fluxes and oceanic mixing from the  $^{10}\text{Be}/^{9}\text{Be}$  ratio: Implications for sedimentary records, *Geophys*  
 620 *Res Lett*, 44, <https://doi.org/10.1002/2017GL074259>, 2017.

621 Wollenburg, J. E. and Kuhnt, W.: The response of benthic foraminifers to carbon flux and primary production in  
 622 the Arctic Ocean, in: *Marine Micropaleontology*, [https://doi.org/10.1016/S0377-8398\(00\)00039-6](https://doi.org/10.1016/S0377-8398(00)00039-6), 2000.

623 Wollenburg, J. E. and Mackensen, A.: On the vertical distribution of living (Rose Bengal stained) benthic  
 624 foraminifers in the Arctic Ocean, *J Foraminifer Res*, 28, <https://doi.org/10.2113/gsjfr.28.4.268>, 1998.

625 Wollenburg, J. E., Matthiessen, J., Vogt, C., Nehrke, G., Grotheer, H., Wilhelms-Dick, D., Geibert, W., and  
 626 Mollenhauer, G.: Omnipresent authigenic calcite distorts Arctic radiocarbon chronology, *Commun Earth*  
 627 *Environ*, 4, <https://doi.org/10.1038/s43247-023-00802-9>, 2023.

628 Yiou, F., Raisbeck, G. M., Baumgartner, S., Beer, J., Hammer, C., Johnsen, S., Jouzel, J., Kubik, P. W.,  
 629 Lestringuez, J., Stiévenard, M., Suter, M., and Yiou, P.: Beryllium 10 in the Greenland Ice Core Project ice core  
 630 at Summit, Greenland, *J Geophys Res Oceans*, 102, <https://doi.org/10.1029/97JC01265>, 1997.

631 Zheng, M., Liu, H., Adolphi, F., Muscheler, R., Lu, Z., Wu, M., and Prisle, N. L.: Simulations of  $^7\text{Be}$  and  $^{10}\text{Be}$   
 632 with the GEOS-Chem global model v14.0.2 using state-of-the-art production rates, *Geoscientific Model*  
 633 *Development Discussions*, <https://doi.org/10.5194/gmd-2023-111>, 2023.

634